NANO LETTERS

Letter

pubs.acs.org/NanoLett

Brownian Motion in a Designer Force Field: Dynamical Effects of Negative Refraction on Nanoparticles

A. Cuche, B. Stein, A. Canaguier-Durand, E. Devaux, C. Genet,* and T. W. Ebbesen

ISIS & icFRC, University of Strasbourg and CNRS, 8 allée Gaspard Monge, 67000 Strasbourg, France

Supporting Information

ABSTRACT: Photonic crystals (PC) have demonstrated unique features that have renewed the fields of classical and quantum optics. Although holding great promises, associated mechanical effects have proven challenging to observe. We demonstrate for the first time that one of the most salient properties of PC, namely negative refraction, can induce specific forces on metal nanoparticles. By integrating a periodically patterned metal film in a fluidic cell, we show that near-field optical forces associated with negatively refracted surface plasmons are capable of controlling particle trajectories. Coupling particle motions to PC band structures draws new approaches and strategies for parallel and high resolution all-optical control of particle flows with applications for micro- and nanofluidic systems.

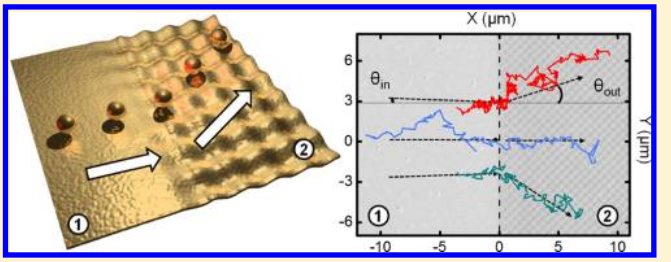

KEYWORDS: *Optical forces, Brownian motion, surface plasmons, microfluidics, negative refraction, optical sorting*

Optical Bloch modes of photonic crystals (PC) follow dispersion relations $\omega(\mathbf{k})$ which, under monochromatic excitation at frequency ω, correspond in the reciprocal $\mathbf{k}$ space to isofrequency surfaces (IFS).[1] The periodic spatial modulation of the crystal opens gaps in $\omega(\mathbf{k})$, an effect that has been discussed both in the context of PC and surface plasmons (SP).[2,3] Salient too is the fact that the group velocity of a Bloch mode $\mathbf{v}_g(\mathbf{k}) = \nabla_k\omega(\mathbf{k})$ is perpendicular to the IFS and is directed along the time-averaged Poynting vector of the Bloch mode, integrated over the unit cell of the PC. The outstanding optical properties of PC stem from the control of IFS given through structural design. Among these, the phenomenon of negative refraction has been recognized as one of the most important[4−6] and hence thoroughly explored in a number of milestone experiments.[7−10] Recently, we have shown how these discussions can be transferred to SP optics and how plasmonic crystals (PlC) share the same unique features of PC.[11] We demonstrate for the first time how these concepts can be further extended to the field of light-induced forces, with new dynamical effects probed in a microfluidic environment.

Direct manipulation of particles through light-induced forces is most efficient in low-Reynolds number fluids because of buoyancy and reduction of inertial effects with tremendous impact on physics, chemistry, and life sciences.[12−14] Conventional techniques unfortunately turn out being rapidely limited at the nanoscale due to light diffraction. This triggered the development of alternative approaches based on near-field optical interactions.[15−20] In this context, our work presents a new strategy for all-optical control of nanoparticle motion in fluids based on tailored SP modes. It offers an all-optical nanoparticle angular sorting method characterized by high-angular resolutions together with high throughputs. Operating on a large scale, our method is not limited by the usual tight focusing requirements of optical tweezer-based manipulations. Because it does not resort to any tags or other markers, our strategy is potentially relevant given the strong current interest in designing new passive sorting techniques.[21]

Confined along a metal/fluid interface, an SP mode is described by a complex in-plane $\mathbf{k}_{\|}$ wave vector along the real part of which the mode propagates.[22] In a plasmonic field of frequency ω and transverse wave vector $k = (\varepsilon_{\text{fluid}})^{1/2}\omega/c$ extending in the fluid, metallic nanoparticles experience time-averaged forces that combine a gradient contribution and an extinction contribution also known as radiation pressure.[23,24] Up to a term negligible given our experimental configuration (see Supporting Information), the extinction contribution $\mathbf{F}_{\text{ext}}$ writes as

$$\mathbf{F}_{\text{ext}} = \left(\frac{2}{3}k^3|\alpha_0|^2 + \text{Im}(\alpha_0)\right)\omega\mathbf{S} \tag{1}$$

accounting for the coupling between the field and the dipolar moment of the nanoparticle of α_0 polarizability (Clausius-Mossotti). The first and second terms represent respectively scattering and absorbing components, both proportional to the time-averaged SP Poynting vector $\mathbf{S}$ which therefore determines the orientation of the extinction force. With an in-plane component of $\mathbf{S}$ along their in-plane propagation direction $\text{Re}[\mathbf{k}_{\|}]$, SP modes have been demonstrated to push efficiently, but only unidirectionally, metallic particles.[25] While similar effects can be observed using dielectric nanoparticles, they are

Received: May 31, 2012
Revised: July 10, 2012

dx.doi.org/10.1021/nl302060t | *Nano Lett.* XXXX, XXX, XXX−XXX

however optimally accessible using metallic nanoparticles because of the strength of the scattering component associated with a metallic polarizability.

The key aspect of our work is that in a PlC, the relation built on the group velocity $\mathbf{v}_g = \nabla_k\omega(\mathbf{k})$ between the Poynting vector of the SP Bloch mode $\mathbf{S}$ and the IFS becomes, through that same Poynting vector, a relation between the IFS and the orientation of the extinction force $\mathbf{F}_{ext}$ of the SP Bloch mode exerted on metallic particles. IFS design is thus a very efficient tool for all-optical control of particle trajectories in the near-field.

To evidence this, we performed a series of experiments on a colloidal suspension of gold nanoparticles immersed in water above a thin gold film. A doubly periodic grating of sinusoidal profiles was fabricated on a given region of the film (region 2 hereafter). SP modes were launched from an unstructured region of the metal/water interface (region 1) and made propagate toward the PlC (see Supporting Information). We used a λ_L = 980 nm laser beam and gold nanoparticles of 250 nm diameter so that the colloidal extinction peak is located on the blue side but close to λ_L. In this case, scattering contributions dominate, aligning forces along the SP Poynting vector, while additional gradient SP forces point toward the metal surface. Figures 1C,D show metallic nanoparticles propelled by SP modes from unstructured to PlC regions.

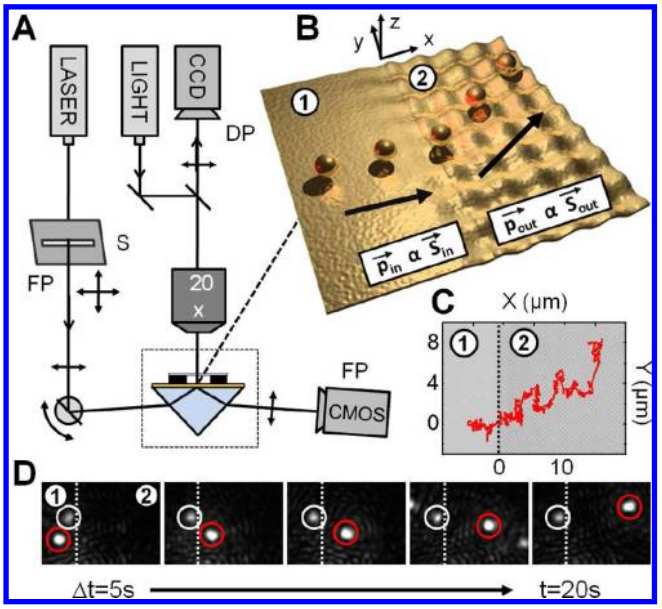

Figure 1. (A) Schematic of the setup with the movable filtering slit (S) in the Fourier plane (FP), and the Fourier and direct plane (DP) detectors. (B) Close-up representation of the metallic nanoparticles moving in the fluidic cell above the metal film from the unstructured region 1 to the patterned PlC region 2. (C) Experimental trajectory of a gold nanoparticle crossing the PlC interface with incident k_y = 0.184 μm^{-1}. (D) Associated dark-field video acquisitions of the moving particle (red circle) referenced to a fixed particle on the surface (white circle).

We have designed the PlC in such a way as to present an IFS with inverted curvature between the band gaps (Figure 2A) that leads to SP negative refraction.[11] In order to probe this IFS region with sufficient resolution, we launched a practically collimated SP mode on the planar region of the film and made it propagate toward the PlC at a given incident angle set by the value of the k_y component of the incident SP wave

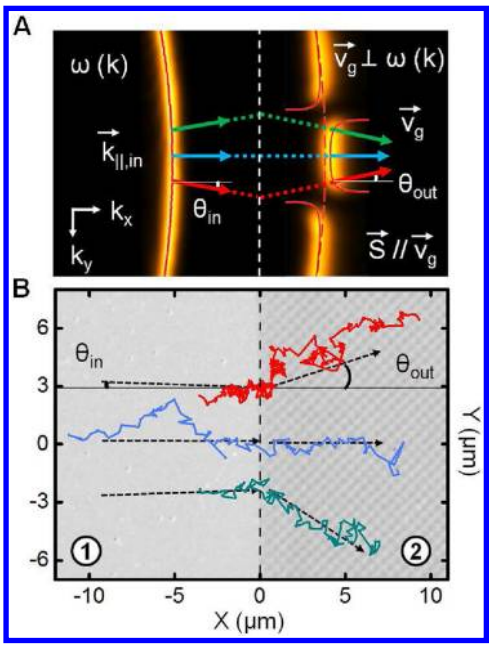

Figure 2. (A) Plasmonic IFS $\omega(\mathbf{k})$ imaged in the Fourier space (FS) associated with regions 1 and 2. Calculated dispersion relations are superimposed as red lines (see Supporting Information text S1). (B) Experimental real space trajectories of particles crossing the interface between region 1 and 2 for three different choices of the SP beam incident angle.

vector $\mathbf{k}_{||,in} = k_x\hat{\mathbf{x}} + k_y\hat{\mathbf{y}}$. Details are given in the Supporting Information. This mode excites an SP Bloch mode at the PlC interface that is negatively refracted for any nonzero value of k_y between the band gaps (Figure 2A).

We recorded the trajectories of single nanoparticles which were first unidirectionally propelled toward the PlC by an SP mode on region 1 and then conveyed by the SP Bloch mode excited at the PlC interface (Figure 2B). When entering region 2, each particle is steered in consistency with angles expected from the intersection between the IFS and the k_y value. Fixing k_y within the relevant regions of the IFS, we observed that the nanoparticle is negatively routed just like the SP mode is negatively refracted when entering the PlC.

These dynamical effects are clearly intertwined with natural Brownian motion of the immersed nanoparticles, characterized by a friction coefficient γ and a fluctuating force that maintains thermal energy k_BT in the fluid. For a gold nanoparticle of mass m in water, friction prevails over inertia by several order of magnitudes, considering the high rate $\gamma/m \sim 10^7 s^{-1}$ of kinetic energy loss through friction. The constant optical extinction force results therefore in a ballistic motion associated with a constant averaged in-plane momentum $\bar{\mathbf{p}} = (m/\gamma)\mathbf{F}_{ext}$ given to the nanoparticle. Because $\mathbf{F}_{ext} \propto \mathbf{S}$, the in-plane component of this momentum is oriented along the SP in-plane propagation direction.

The introduction of the PlC interface is thus seen as imprinting a momentum discontinuity in the motion of the nanoparticles from both sides of the interface. This can be framed into a dynamical law of refraction

$$\hat{\bar{\mathbf{p}}}_{out} - \hat{\bar{\mathbf{p}}}_{in} = \hat{\mathbf{v}}_g - \hat{\mathbf{k}}_{||,in} \quad (2)$$

in units of momentum, with unit wave vector $\hat{\mathbf{k}}_{||,in}$ and unit group velocity vector $\hat{\mathbf{v}}_g$ locally evaluated on the IFS from the conservation of k_y. Given the fact that $\hat{\mathbf{v}}_g - \hat{\mathbf{k}}_{||,in} = \sin\theta_{out} -$

dx.doi.org/10.1021/nl302060t | Nano Lett. XXXX, XXX, XXX–XXX

sin θ_{in} for the SP beams, our data demonstrate how the IFS structure is mapped onto the nanoparticle motions and confirm eq 2 (Figure 2B).

In terms of a steering angle $\theta_S = \theta_{out} - \theta_{in}$, eq 2 writes as $\sin\theta_S = (\hat{\mathbf{p}}_{in} \times \hat{\mathbf{p}}_{out}) \cdot \hat{\mathbf{z}}$. As seen in Figure 2B, nanoparticle steering angles are opposite in sign and larger in magnitude than the incidence angles for non-normal incidences. This is the clear proof of a mechanical effect due to negative refraction, based on a dynamical transfer from SP fields to nanoparticle motions. Since negative routing is observed for both positive and negative k_y values, this is the exact dynamical replicate of the "all-angle" negative refraction phenomenon in PC.[26]

Similar observations can be made for an ensemble of nanoparticles interacting with the near-field of an extended PlC with motional evolutions again determined in strict relation with the IFS (Figure 3). Our results attest that particle trajectories can be distributed over wide angular sector (±35°) within a range of small incidence angles (±2°) due to the strong local anisotropy of the IFS. In this sense, we demonstrate here the mechanical analog of the superprism effect in PC.[27] We note that thinner fluidic cells, preventing from convection and decoupling effects, would lead to observing much longer trajectories.

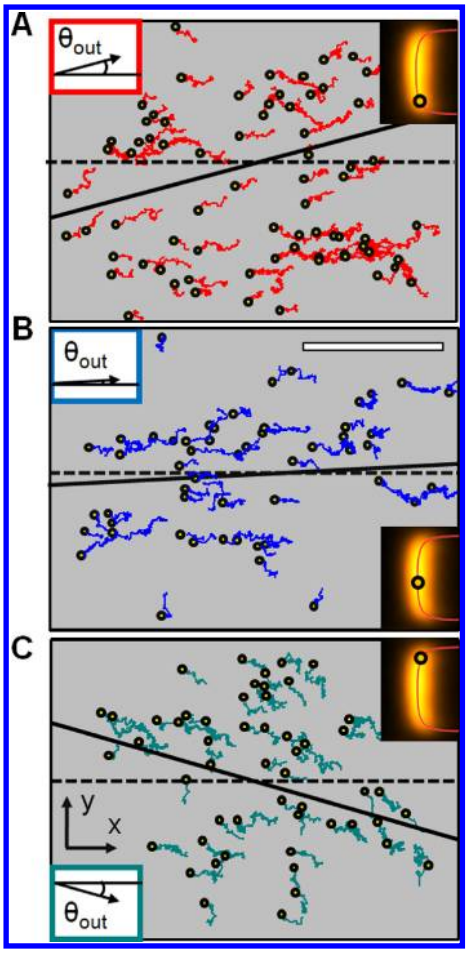

Figure 3. Experimental ensembles of nanoparticle trajectories (starting positions shown as open circles) recorded on the PlC (region 2) showing parallel motions for three specific points on the IFS of the PlC, shown in the insets. These points correspond to three different angles θ_{out} = 14.17° (A), 3.45° (B) and −16.11° (C), directing the motions. Scale bar is 50 μm.

Additionally, our methodology addresses another current issue of microfluidics. Indeed, while high throughputs and high resolution are critical demands put on present microfluidic system designs, they are yet recognized as extremely difficult to achieve simultaneously.[28] In this respect, our large scale experiments (Figure 3) actually reveal that high throughputs have been reached all the while offering high angular sorting resolutions. As gold can be easily functionalizable, our method is also potentially interesting in the context of chemical and biological analysis.[12]

To perform the quantitative analysis of our data, we looked at the nanoparticle trajectories from first principles. In this frame, we treated as a statistical ensemble all the N in-plane elementary particle displacements $\Delta\mathbf{r} = \mathbf{r}(t + \Delta t) - \mathbf{r}(t)$ during a time Δt (fixed to 10 ms in our experiments) gathered from all the trajectories j recorded over a time $T_j = N_j \times \Delta t$ with $N = \Sigma_j N_j$ for a given value of k_y. In a field of constant force, the whole probability distribution of the free Brownian displacements is translated in the $(\Delta x, \Delta y)$ plane[29] (see Supporting Information). This translation corresponds to a ballistic shift of the expectation value of the distribution $\mu = \Delta\bar{\mathbf{r}} = (\mathbf{F}_{ext}\Delta t)/\gamma$, keeping the variance $\sigma^2 = (4k_BT\Delta t)/\gamma$ unchanged. This approach allows determining, within expectation intervals, the angle $\theta_{out} = \arctan(\overline{\Delta y}/\overline{\Delta x})$ along which the extinction force conveys the particles.

The results extracted from this statistical analysis are gathered and presented in Figure 4. Remarkably, they are in close agreement with the IFS of the PlC as experimentally observed. They quantitatively and definitely validate the relation presented in eq 2 and complete the experimental

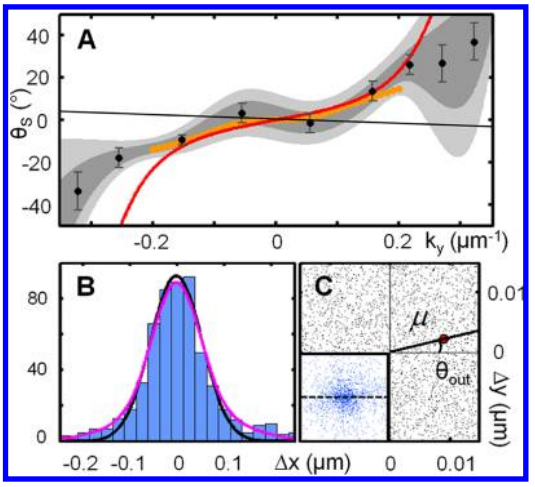

Figure 4. (A) Nanoparticle steering angles (black dots) measured as a function of k_y. Error bars are related to experimental reproducibility. Relations to the IFS of the PlC are shown as a red continuous line for theoretical IFS and as orange dots for the experimentally measured IFS. Statistical confidence intervals are also displayed as colored surfaces for σ_{θ_S} (dark gray) and $2\sigma_{\theta_S}$ (light gray). Comparison with $\theta_{in}(k_y)$ (continuous dark line) reveals the dynamical negative refraction and superprism effects. (B) Displacement probability distribution along the x-axis for k_y = 0.157 μm^{-1}, compared to a Gaussian fit (dark blue curve) and a multi-Gaussian fit (pink curve) in better agreement. (C) Extraction of the ballistic shift $|\mu|$ and the θ_{out} angle from the location of the mean value (red dot) of the displacement distribution in the $(\Delta x,\Delta y)$ plane with respect to free Brownian motion (centered at $\Delta x = \Delta y = 0$). The distribution is zoomed-in from the whole distribution (inset) cross-sected along the x axis in (B).

dx.doi.org/10.1021/nl302060t | Nano Lett. XXXX, XXX, XXX−XXX

demonstration of particle trajectories driven by negative refraction. Note that the deviations of the data points with respect to the calculated IFS at large $|k_y|$ are only due to the finite width of the filtering slit.

While our method can potentially give the intensity of the extinction force from a simple measurement of the shift length $|\mu|$, it is important to stress that the extinction force depends exponentially on the particle height z. Thus, and in contrast with θ_S, $|\mathbf{F}_{ext}|$ is not a constant of motion, as particles also move along the z axis (through axial Brownian motion, gradient forces, gravity, convection, etc.). Our experiments can only probe an effective driving strength of the extinction force, for a given value of k_y.

Accordingly, the statistical precision on θ_S is situation-dependent, related to the strength $|\mu|$ of the effective drive, the variance σ^2 of the Brownian motion, and the number N of elementary displacements considered. Confidence intervals $\sigma_{\theta_S} = \sigma/(|\mu|\sqrt{N})$ evaluated for each data set obtained for each k_y value appear to provide a good statistical resolution criterium (see Supporting Information). This confirms the reliability of the experimental determination of the steering angles θ_S (Figure 4A). Finally, the deviations from the normal law, systematically observed for the displacement distribution (Figure 4B), are due to the vicinity of the surface, perturbing the Brownian motion from thermal effects and modification of the friction coefficient γ[30,31] (see Supporting Information). This issue is however only related to the shape of the distributions and does not affect the expected steering angles θ_S (Figure 4C).

To conclude, our observations and analysis demonstrate the possibility of driving mechanically nanoparticles from the optical band structures of a PC. Exploiting the dynamical action of negative refraction opens perspectives as intriguing as in optics. Given the richness of the optical properties of PC, such results should stimulate the further use and study of opto-mechanical phenomena in micro- and nanofluidic contexts.

■ ASSOCIATED CONTENT

Supporting Information

Further details are provided related to the experimental setup, sample fabrication, particle motion detection strategies, and to the evaluations of time-averaged optical forces and IFS of the plasmonic crystal. A complete theoretical analysis of Brownian motion in a force field is performed together with a statistical evaluation of the experimental resolution. A brief discussion is also given on observed deviations from the normal law for the displacement probability distribution of nanoparticles. This material is available free of charge via the Internet at http://pubs.acs.org.

■ AUTHOR INFORMATION

Corresponding Author

*E-mail: genet@unistra.fr.

Notes

The authors declare no competing financial interest.

■ ACKNOWLEDGMENTS

This work was supported by the European Research Council (Grant 227557). The authors are grateful to H. Majjad for helping with the sample preparation.

■ REFERENCES

(1) Joannopoulos, J. D.; Johnson, S. G.; Winn, J. N; Meade, R. D. *Photonic Crystals: Molding the Flow of Light*; Princeton University Press: Princeton, NJ, 2008.
(2) Glass, N. E.; Weber, M.; Mills, D. L. *Phys. Rev. B* **1984**, *29*, 6548−6559.
(3) Kitson, S. C.; Barnes, W. L.; Sambles, J. R. *Phys. Rev. Lett.* **1996**, *77*, 2670−2673.
(4) Pendry, J. B. *Contemporary Phys.* **2004**, *45*, 191−202.
(5) Yao, J.; Liu, Z.; Liu, Y.; Wang, Y.; Sun, C.; Bartal, G.; Stacy, A. M.; Zhang, X. *Science* **2008**, *321*, 930.
(6) Yu, N.; Genevet, P.; Kats, M. A.; Aieta, F.; Tetienne, J.-P.; Capasso, F.; Gaburro, Z. *Science* **2011**, *334*, 333−337.
(7) Notomi, M. *Phys. Rev. B* **2000**, *62*, 10696−10705.
(8) Luo, C.; Johnson, S. G.; Joannopoulos, J. D.; Pendry, J. B. *Opt. Express* **2003**, *11*, 746−754.
(9) Cubukcu, E.; Aydin, K.; Ozbay, E.; Foteinopoulou, S.; Soukoulis, C. M. *Nature* **2003**, *423*, 604−605.
(10) Ni, X.; Emani, N. K.; Kildishev, A. V.; Boltasseva, A.; Shalaev, V. M. *Science* **2012**, *335*, 427.
(11) Stein, B.; Laluet, J.-Y.; Devaux, E.; Genet, C.; Ebbesen, T. W. *Phys. Rev. Lett.* **2010**, *105*, 266804−266807.
(12) Fan, X.; White, I. M. *Nat. Photonics* **2011**, *5*, 591−597.
(13) Schmidt, H.; Hawkins, A. R. *Nat. Photonics* **2011**, *5*, 598−604.
(14) Monat, C.; Domachuk, P.; Grillet, C.; Collins, M.; Eggleton, B. J.; Cronin-Golomb, M.; Mutzenich, S.; Mahmud, T.; Rosengarten, G.; Mitchell, A. *Microfluid. Nanofluid.* **2008**, *4*, 81−95.
(15) Kawata, S.; Sugiura, T. *Opt. Lett.* **1992**, *17*, 772−774.
(16) Ng, L. N.; Luff, B. J.; Zervas, M. N.; Wilkinson, J. S. *Opt. Commun.* **2002**, *208*, 117−124.
(17) Juan, M. L.; Righini, M.; Quidant, R. *Nat. Photonics* **2011**, *5*, 349−356.
(18) Yang, A. H. J.; Lerdsuchatawanich, T.; Erickson, D. *Nano Lett.* **2009**, *9*, 1182−1188.
(19) Erickson, D.; Serey, X.; Chen, Y.-F.; Mandal, S. *Lab Chip* **2011**, *11*, 995−1009.
(20) Cuche, A.; Mahboub, O.; Devaux, E.; Genet, C.; Ebbesen, T. W. *Phys. Rev. Lett.* **2012**, *108*, 026801−026804.
(21) Ploschner, M.; Cizmar, T.; Mazilu, M.; Di Falco, A.; Dholakia, K *Nano Lett.* **2012**, *12*, 1923−1927.
(22) Drezet, A.; Hohenau, A.; Koller, D.; Stepanov, A.; Ditlbacher, H.; Steinberger, B.; Aussenegg, F. R.; Leitner, A.; Krenn, J. R. *Mater. Sci. Eng., B* **2008**, *149*, 220−229.
(23) Chaumet, P. C.; Nieto-Vesperinas, M. *Opt. Lett.* **2000**, *25*, 1065−1067.
(24) Stenholm, S. *Rev. Mod. Phys.* **1986**, *58*, 699−739.
(25) Wang, K.; Schonbrun, E.; Crozier, K. B. *Nano Lett.* **2009**, *9*, 2623−2629.
(26) Luo, C.; Johnson, S. G.; Joannopoulos, J. D.; Pendry, J. B. *Phys. Rev. B* **2002**, *65*, 201104−201107(R).
(27) Kosaka, H.; Kawashima, T.; Tomita, A.; Notomi, M.; Tamamura, T.; Sato, T.; Kawakami, S. *Phys. Rev. B* **1998**, *58*, 10096−10099(R).
(28) Chiou, P. Y.; Ohta, A. T.; Wu, M. C. *Nature* **2005**, *436*, 370−372.
(29) Uhlenbeck, G. E.; Ornstein, L. S. *Phys. Rev.* **1930**, *36*, 823−841.
(30) Carbajal-Tinoco, M. D.; Lopez-Fernandez, R.; Arauz-Lara, J. L. *Phys. Rev. Lett.* **2007**, *99*, 138303−138306.
(31) Volpe, G.; Helden, L.; Brettschneider, T.; Wehr, J.; Bechinger, C. *Phys. Rev. Lett.* **2010**, *104*, 170602−170605.